

# Effects of the subtropical anticyclones over North Africa and Arabian Peninsula on the African easterly jet

James Spinks,<sup>a</sup> Yuh-Lang Lin<sup>a,b\*</sup> and Ademe Mekonnen<sup>a</sup>

<sup>a</sup> Department of Energy and Environmental Systems, North Carolina A&T State University, Greensboro, NC, USA

<sup>b</sup> Department of Physics, North Carolina A&T State University, Greensboro, NC, USA

**ABSTRACT:** North African climate is analysed between 1979 and 2010 with an emphasis on August using the European Center for Medium-Range Weather Forecast (ECMWF) global dataset to investigate the effects of the subtropical anticyclones over North Africa and the Arabian Peninsula on the African easterly jet (AEJ). It was found that the AEJ encloses a core with a local wind maximum (LWM) in both West and East Africa, in which the west LWM core has a higher zonal wind speed. The strength of both cores is distinctly different by way of thermal wind balance. As found in previous studies, the AEJ is formed through baroclinicity with influence from Saharan lower level heating along and to the north of the Intertropical Front (ITF). As there are two separate anticyclonic centres, the AEJ is maintained by the anticyclonic systems in West Africa, East Africa as well as the Arabian Peninsula. The presence of these two anticyclonic centres provides the AEJ with two separate core maxima with the western LWM located at 15°W, 17°N and the eastern LWM located at 35°E, 15°N for August.

**KEY WORDS** African easterly jet; African easterly wave; local wind maximum; East Africa; Arabian Peninsula; Sahara Desert; ECMWF; Ethiopian Highlands

Received 7 April 2013; Revised 18 March 2014; Accepted 21 March 2014

## 1. Introduction

The African easterly jet (AEJ) is a synoptic feature over North Africa, which is a localized wind maximum embedded in an easterly wind flow in the mid-troposphere at 600 mb. Several questions regarding the roles played by the AEJ contributing to North African climate and weather have been raised in the past. A number of studies have been devoted to achieve a better understanding of the formation and maintenance of the AEJ, but most of the research has been performed in West Africa. For example, Cook (1999) examined the dynamics of the AEJ whereas Thorncroft and Blackburn (1999) and Chen (2005) investigated the maintenance of the AEJ. Very few studies of AEJ are focused on East Africa, which is the focus of this study.

Dezfuli and Nicholson (2010) investigated the structure of the AEJ over a 56-year period and examined a second wind maximum of the AEJ located in East Africa around 20°E, whose amplitude varies per year for the month of August. A careful inspection of the 56-year long mean of the AEJ in Figure 1 from Dezfuli and Nicholson (2010) reveals that a second maximum exists further east of 30°E; however, the authors noted that a second maximum does not exist in the long-term mean of the AEJ. In contrast, Cook (1999) did a comparison of the European Centre Medium-Range Weather Forecast (ECMWF) 40-Year Reanalysis (ERA-40) (Uppala *et al.*, 2005) and National

Center of Environmental Prediction (NCEP) reanalysis (Kalnay *et al.*, 1996) data analysing the AEJ and there was a second wind maximum located around 40°E in the ERA-40 data, but the author did not address the second wind maximum.

In this study, we will address the AEJ and its two wind maximums over East Africa, West North Africa and the Arabian Peninsula for 32 years of August between 1979 and 2010 and 2006 as a case study. We will also explore the dynamics of the Saharan and Arabian Highs, and why the East local wind maximum (denoted as LWM<sub>E</sub> hereafter) is weaker than the West LWM (denoted as LWM<sub>W</sub> hereafter). August was chosen because it is the peak rainfall month over East Africa.

## 2. Background

The AEJ is located between dry Saharan (20°–35°N) and moist tropical (5°–20°N) regions. The AEJ lies between 600 and 700 mb and exists as a result of the thermal wind balance with positive meridional temperature gradient (Cook, 1999; Thorncroft and Blackburn, 1999; Parker *et al.*, 2005). Grist *et al.* (2002) observed the mean speed of the LWM<sub>W</sub> for the month of August to be 10–12 m s<sup>-1</sup>. Another observation was from the Jet2000 project (Thorncroft *et al.*, 2003) that examined the LWM<sub>W</sub> as a synoptic event to have a much stronger zonal speed of 21 m s<sup>-1</sup>, which was higher than the climatological average value of 15 m s<sup>-1</sup> (e.g. Reed *et al.*, 1977). Dezfuli and Nicholson (2010) observed the LWM<sub>W</sub> to have a mean speed of

\* Correspondence to: Y.-L. Lin, 302H Gibbs Hall, EES, North Carolina A&T State University, 1601 E. Market St., Greensboro, NC 27411, USA. E-mail: ylin@ncat.edu

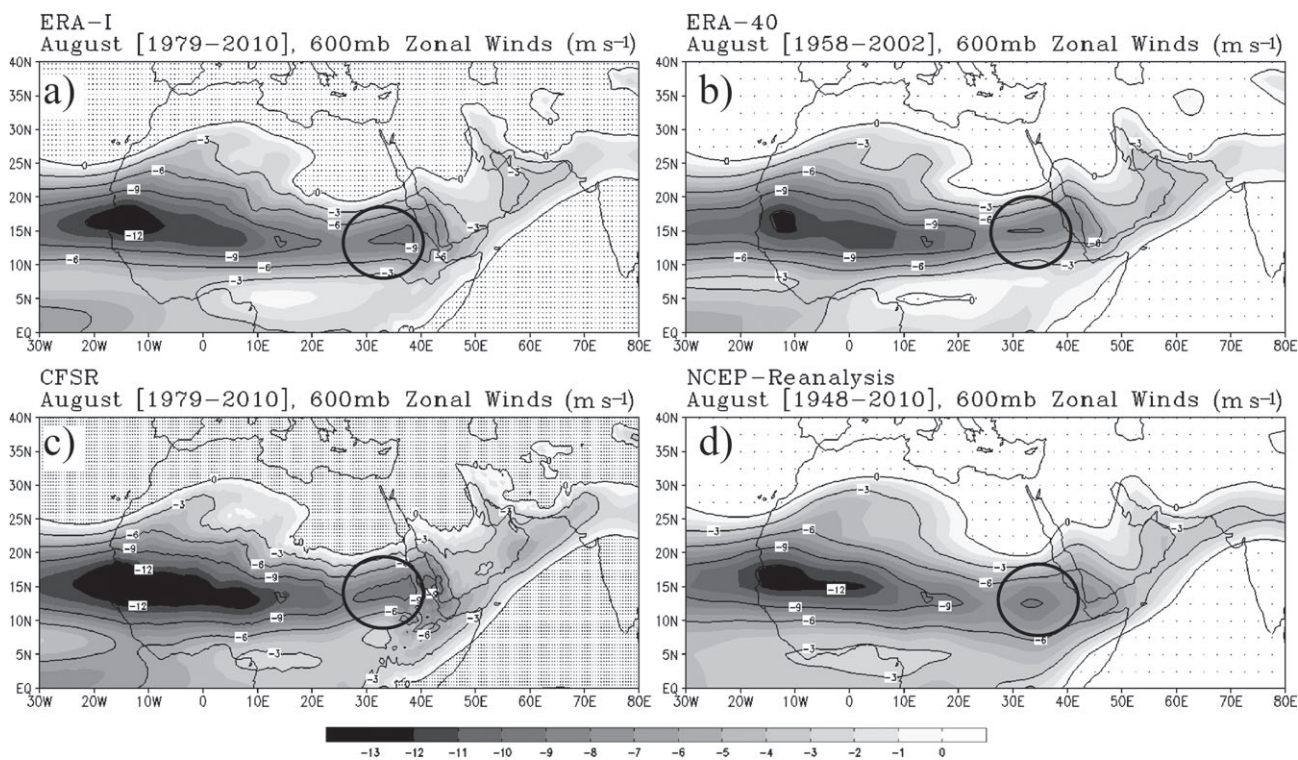


Figure 1. The 600 mb zonal wind is depicted to show the local wind maximum east (black circle) in different datasets. The shade is for easterly winds every  $1 \text{ m s}^{-1}$ , the contours are easterly winds every  $3 \text{ m s}^{-1}$ , and the stippling indicates grid spacing of respected dataset for westerly winds. (a) The European Centre Medium-Range Weather Forecast Intermediate reanalysis on a  $0.75^\circ$  grid with zonal averages for the month of August between 1979 and 2010. (b) The European Centre Medium-Range Weather Forecast 40-Year reanalysis on a  $2.5^\circ$  grid with zonal averages for the month August between 1958 and 2002. (c) The Climate Forecasting System (version 1) reanalysis on a  $0.3^\circ$  grid with zonal averages for the month of August between 1948 and 2010. (d) The National Center of Environmental Prediction reanalysis on a  $2.5^\circ$  grid with zonal averages for the month of August between 1979 and 2010.

$13.5 \text{ m s}^{-1}$  and the  $\text{LWM}_E$  to have a mean speed of  $12.7 \text{ m s}^{-1}$ .

The North African climate during summer includes synoptic features that influence the AEJ patterns on the continent, which consist of the Tropical easterly jet (TEJ) in the upper troposphere, the Saharan High in the mid-troposphere, Saharan thermal low in the lower troposphere, and the Inter Tropical Convergence Zone (ITCZ) (Wu *et al.*, 2009). There is also a low-level convergence zone located at  $20^\circ\text{N}$  in North Africa, which is also known as the Intertropical Front (ITF). The maximum vertical motion associated with the ITF is tilted toward the south with height into the mid-troposphere between  $10^\circ$  and  $15^\circ\text{N}$ , which is collocated with the ascending branch of the Hadley Cell. The location of the Hadley Cell ascending branch is where the highest rainfall occurs and is often referred to as the ITCZ.

Warm low-level temperatures dominate the continent causing a rather unstable atmosphere. The cooler temperatures in the tropical region are a result of temperature advection from the Gulf of Guinea due to the African monsoon westerlies. Northward flow onto the continent across the Guinean coast curves eastward to form the equatorward section of cyclonic flow about a thermal low centred over Saharan Africa (Cook, 1999; Lavaysse *et al.*, 2009). The Saharan planetary boundary layer (PBL) affects the

troposphere from the surface up to about 600 mb and can be found along and to the north of the ITF where buoyancy produces vertical motion forcing warm air into the mid-atmosphere and causing convergence at lower levels (Wu *et al.*, 2009). The low-level convergence and upper level divergence over the continent constitute a secondary circulation that concentrates cyclonic vorticity at the lower levels and anticyclonic vorticity at the upper levels (Holton, 2004; Lavaysse *et al.*, 2010).

Chen (2005) described the role that the Saharan High plays on the  $\text{LWM}_W$  intensity by observing the circulation patterns over Africa. The lower tropospheric monsoon southerly flow over West Africa is established by the lower branch of the Hadley circulation. The TEJ in the upper troposphere is located aloft over the equatorward branch of the Hadley circulation, whereas the  $\text{LWM}_W$  is placed over the southward branch of the Saharan circulation. The upward (hot) vertical motion driven by the thermal low heating and the downward (cold) branch of the Indian monsoon form a strong divergence centre. The link between the upper and lower tropospheric circulation over North Africa can be established through this divergence centre. The Saharan High covers most of North Africa between  $20^\circ\text{W}$  and  $20^\circ\text{E}$  between 700 and 400 mb.

This paper is organized as follows: Section 3 will provide the data information used for this study; Section 4 will elaborate the AEJ dynamics and investigate the  $\text{LWM}_E$  and

Arabian High in relation to previous research by authors who investigated the  $LWM_W$  and the Saharan High. This will provide better understanding on the behaviours of the AEJ during its most unstable month of August as well as offer insight on the variability of the synoptic environment that surrounds and affects the AEJ. Concluding remarks can be found in Section 5.

### 3. Data

Over the years, climatological analyses of the AEJ were carried out using global model data with relatively low spatial resolutions. Cook (1999) investigated the AEJ and its formation using the NCEP reanalysis data for the month of July between 1957 and 1996. This dataset consists of a resolution of  $2.5^\circ \times 2.5^\circ$  globally. Chen (2005) used the NCEP reanalysis data for June, July, and August between 1979 and 2002 to study the AEJ in relation to the Saharan High. Chen (2006) also used the ERA-40 dataset with a  $2.5^\circ \times 2.5^\circ$  global grid for the summer months of June, July, August, and September between 1991 and 2000 to examine African easterly waves (AEWs), the AEJ, and Saharan High. Dezfuli and Nicholson (2010) analysed the AEJ using the NCEP reanalysis dataset for the month of August between 1948 and 2003 on a monthly time scale.

In this study, we will use the ECMWF-Interim (ERA-I) reanalysis data with a spatial resolution of  $0.75^\circ \times 0.75^\circ$  global for the month of August between 1979 and 2010 (Dee *et al.*, 2011). The investigation of the AEJ structure and intensity from previous studies that used the NCEP reanalysis or the ERA-40 may vary from this research. Limitations of the NCEP data and ERA-40 would include their lower spatial resolution and the discrepancies of the AEJ intensity.

Figure 1 illustrates the  $LWM_E$  at 600 mb from various datasets to confirm consistency in this feature. The ERA-I and Climate Forecasting System Reanalysis version 1 (CFSR) at  $0.3^\circ$  (Saha *et al.*, 2006) show a clear depiction of the  $LWM_E$  in East Africa (Figure 1(a) and (c)) for the month of August between 1979 and 2010. There is an indication of a very small and weak  $LWM_E$  in the ERA-40 (Figure 1(b)) and NCEP reanalysis (Figure 1(d)) datasets. The weak resolution of the  $LWM_E$  from these respected datasets is due to the size of the  $LWM_E$ . On the basis of ERA-I and CFSR, the  $LWM_E$  is about  $10^\circ$  ( $\sim 1100$  km) in length and  $3^\circ$  in width. With the spatial resolution of the ERA-40 and NCEP reanalysis being  $2.5^\circ$ , this would leave about four grid points for the ERA-40 and NCEP reanalysis to resolve the  $LWM_E$ . The  $LWM_E$  is prominent in all of the presented datasets at 550 and 500 mb (not shown).

### 4. Results

#### 4.1. Synoptic features and circulation over North Africa

To explore the circulation of subtropical anticyclones, we use streamfunction as a diagnostic variable. For the month

of August between 1979 and 2010, the major atmospheric features are depicted in Figure 2. As seen in Figure 2(a), the TEJ axis is located on the southern rim of the Tibetan high with the TEJ intensity decreasing from east to west. The maximum intensity of the TEJ is located to the south of the Tibetan anticyclone centre and extends into the southwestern Arabian Peninsula and East Africa.

At 600 mb (Figure 2(b)), two high pressure systems are shown: the Saharan High around  $10^\circ W, 25^\circ N$  and the other is the Arabian High around  $37^\circ E, 22^\circ N$ . The AEJ axis is located to the south of the anticyclonic circulations around  $17^\circ W-45^\circ E, 10^\circ-20^\circ N$ . The intensity of the  $LWM_E$  at  $35^\circ E, 15^\circ N$  has a zonal wind speed average of  $9.81 \text{ m s}^{-1}$  and the intensity of the  $LWM_W$  at  $17^\circ W, 18^\circ N$  has a zonal wind speed average of  $13.41 \text{ m s}^{-1}$ . Note that the  $LWM_W$  and Saharan High are much stronger than the corresponding  $LWM_E$  and Arabian High.

At 925 mb, two major anticyclonic systems are located over the Atlantic and Indian Oceans. In Figure 2(c), the ITF can be depicted using upward motion ( $-\omega > 0$ ) where there is strong baroclinicity along the convergence zone. Across North Africa at  $20^\circ N$ , the converging winds from the Guinea Monsoon and the northerly Harmattan flow are effects from the generation of the Saharan thermal low ( $15^\circ W, 20^\circ N$ ). Several intense upward motion regions exist across North Africa as part of the ITF heating. There is a strong vertical motion on the lee (west) side of the Darfur Mountains around  $20^\circ E, 20^\circ N$ , on the lee side of the northern most part of the Ethiopian Highlands around  $35^\circ E, 20^\circ N$ , and another over the Asir Mountains around  $43^\circ E, 20^\circ N$ . The vertical motion over the Arabian Peninsula is associated with the Arabian thermal low.

Exploring the east–west circulation will provide insight on how the anticyclonic systems are maintained. The streamlines on a zonal and meridional vertical cross section of North Africa depicts the east–west circulation (Figure 3(a)) along the ITF approximately  $20^\circ N$ , the north–south Hadley Circulation over West Africa ( $10^\circ-15^\circ W$ ) (Figure 3(b)), and the north–south Hadley Circulation over East Africa ( $35^\circ-40^\circ E$ ) (Figure 3(c)). The east–west circulation was computed using the magnitude of zonal winds ( $u$ ) and negative omega ( $-\omega$ ). Figure 3(a) illustrates the upward motion caused by the Saharan thermal heating and Arabian thermal heating along the ITF. Warm air is lifted into the mid-troposphere, in which it will converge with the sinking cooler air from the upper troposphere. The strong divergence from the vertical flow can be seen at the mid-troposphere located between 600 and 400 mb in West Africa and 600–500 mb in East Africa. This indicates that the Arabian High is shallower in comparison with the Saharan High. Similar divergent flows can be found on meridional cross sections averaged between  $10^\circ-15^\circ W$  (Figure 3(b)) and  $35^\circ-40^\circ E$  (Figure 3(c)). Figure 3(b) is a vertical cross section over the Saharan thermal low and Figure 3(c) is a vertical cross section over the Arabian thermal low. Figure 3(b) and (c) is the magnitude of meridional winds ( $v$ ) and negative omega ( $-\omega$ ). The ITCZ is located between the

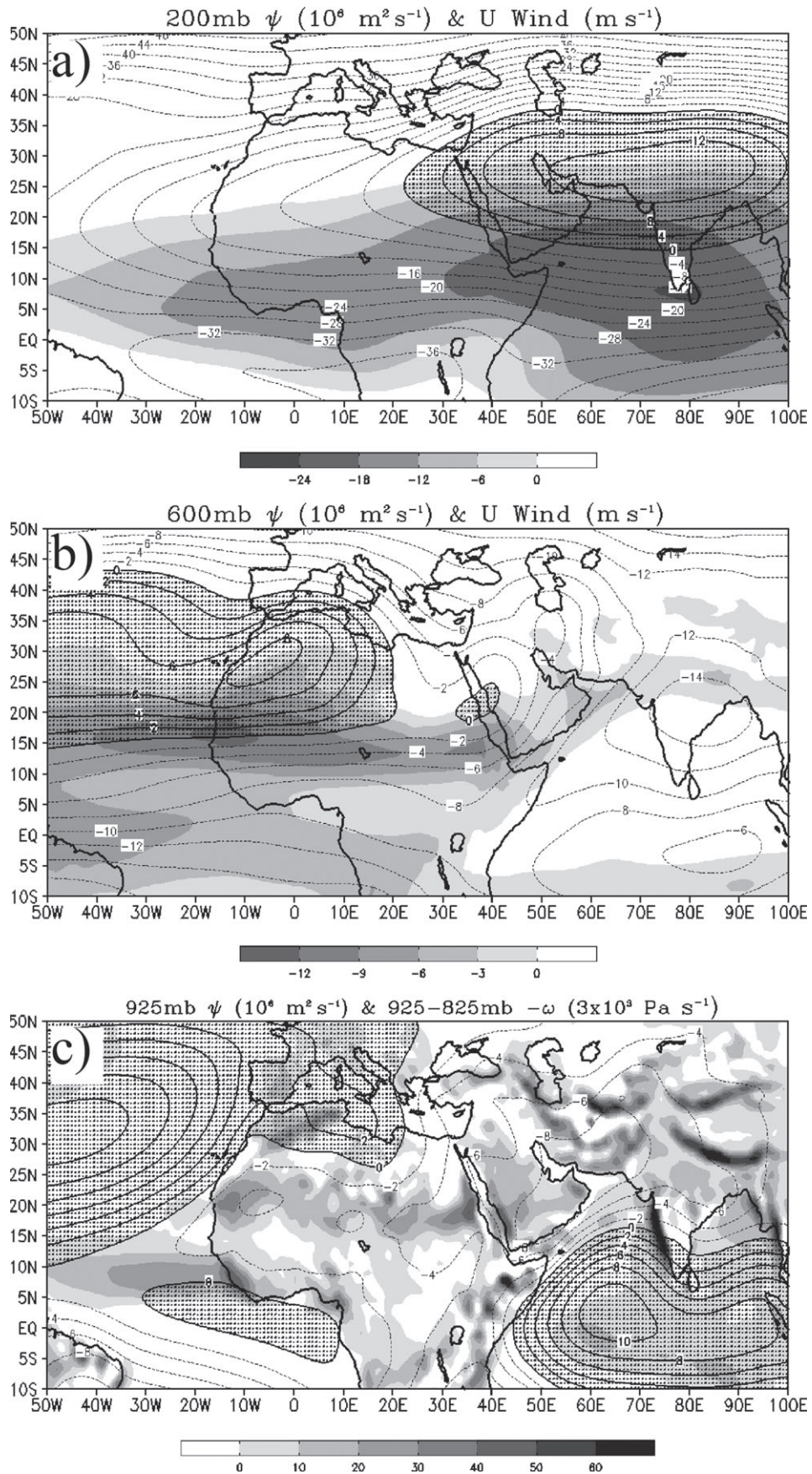


Figure 2. August 32-year (1979–2010) average of (a) 200 mb streamfunction ( $\psi$ ) ( $\times 10^6 \text{ m}^2 \text{ s}^{-1}$ ) contoured every  $2 \text{ m}^2 \text{ s}^{-1}$  and zonal velocity shaded every  $6 \text{ m s}^{-1}$ , (b) 600 mb streamfunction contoured every  $2 \text{ m}^2 \text{ s}^{-1}$  and zonal velocity shaded every  $3 \text{ m s}^{-1}$ , and (c) 925 mb streamfunction contoured every  $2 \text{ m}^2 \text{ s}^{-1}$  and averaged 925–825 mb vertical velocity ( $3 \times 10^3 \text{ Pa s}^{-1}$ ) shaded every  $10 \text{ Pa s}^{-1}$ . The stippling is positive values for streamfunction.

southern Hadley Cell (south of 10°N) and the northern Hadley Cell (north of 10°N) with divergent flow in the upper troposphere. This is consistent with Chen's (2005) findings on the divergent flow from the northern and southern Hadley Cell interaction. The cross section in Figure 3(c) reveals similarities of a divergent flow present in the upper troposphere. There exists a Hadley Cell to the north and south of the ITCZ in the eastern African region. The ITF in East Africa starts in the lower troposphere around 20°N, and then tilts to the south around 12°N in the mid-troposphere where the strongest vertical motions are located.

To get a better understanding of the flow field across North Africa at 600 mb, the streamfunction (Figure 2(b)) and velocity potential fields (Figure 4) have been compared. The streamfunction field shows the rotational flow of the Saharan and Arabian Highs. Between these two anticyclones is a trough located around 25°N, 30°E. On the east side of the Saharan and Arabian Highs are northerly flows that advect hot and dry air into latitudes lower than 20°N. The velocity potential maxima are located to the southeast of the Sahara Desert centre and south of the

Arabian High centre (Figure 4). These divergent centres are formed and maintained from the east–west differential heating induced by the upward branch of the Saharan thermal low and Arabian thermal low heating and cooling from the downward branch of the TEJ, as shown in Figure 3(a) from the east–west circulation. This east–west differential heating serves as a maintenance mechanism for the Saharan and Arabian Highs.

The divergent centre over the Arabian Peninsula is more intense than the divergent centre over Central Sahara as the temperatures and vertical velocities over the Arabian Peninsula are higher than the Saharan Desert (Figure 5). The Arabian thermal heating influences the northerly 'Shamal' wind (e.g. Rao *et al.*, 2003; Lin *et al.*, 2013) and is affected by the southwesterly Somali jet (Hurlburt and Dana Thompson, 1976) from Northern Indian Ocean. These winds converge on the east side of the Asir Mountains in the vicinity of the ITCZ. The vertical motion from the Arabian thermal heating is just as intense as the vertical motion associated with the Saharan thermal heating, but with the exception of higher temperatures over the Arabian Peninsula.

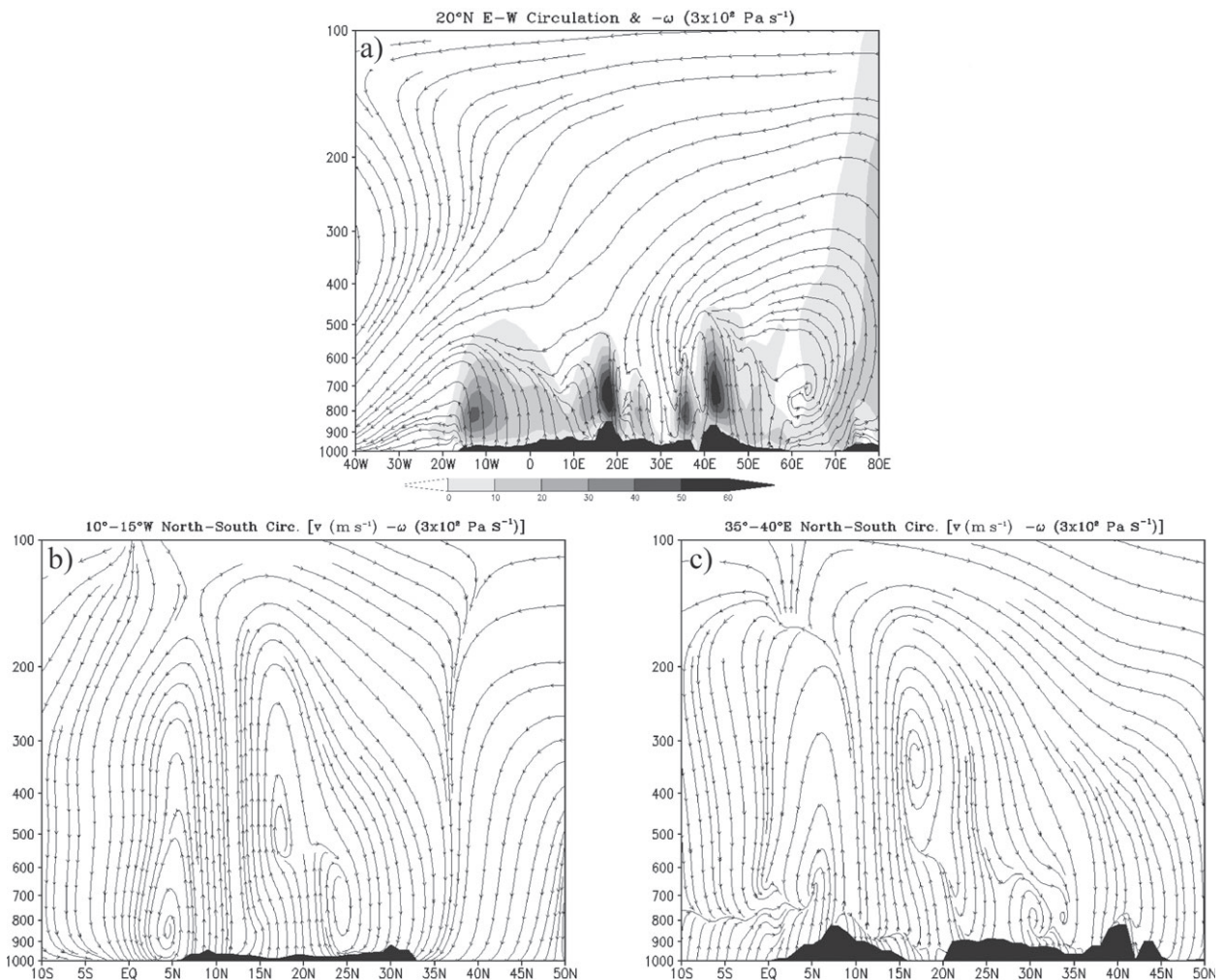


Figure 3. August 32-year (1979–2010) average of (a) zonal vertical cross section at 20°N of  $u$  and  $-\omega$  ( $3 \times 10^2 \text{ Pa s}^{-1}$ ), (b) meridional vertical cross section of  $v$  ( $\text{m s}^{-1}$ ) and  $-\omega$  ( $3 \times 10^2 \text{ Pa s}^{-1}$ ) along 10°–15°W, and (c) meridional vertical cross section along 35°–40°E of  $v$  ( $\text{m s}^{-1}$ ) and  $-\omega$  ( $3 \times 10^2 \text{ Pa s}^{-1}$ ).

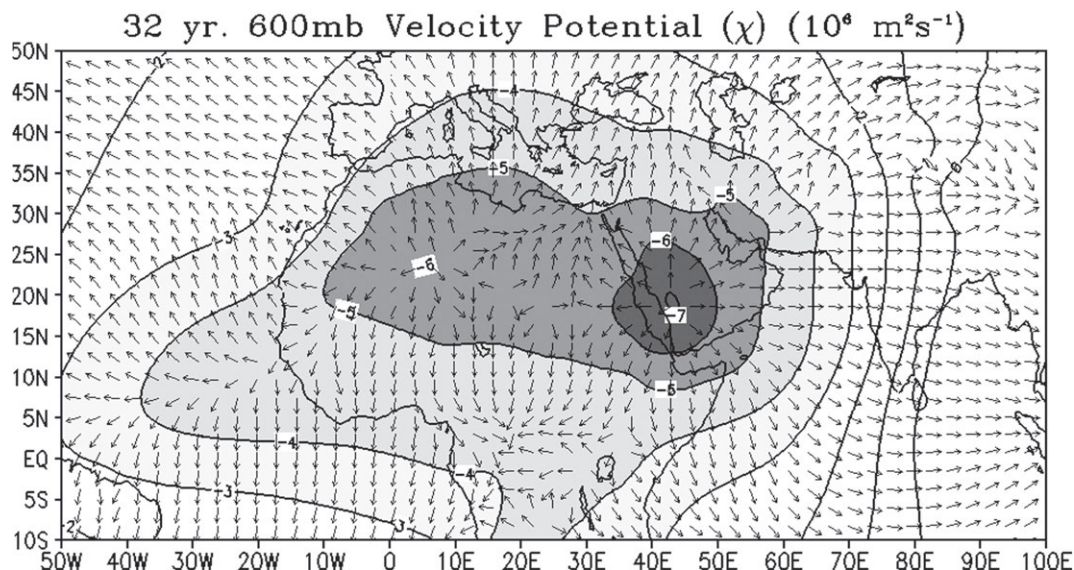


Figure 4. August 32-year (1979–2010) average of 600 mb velocity potential ( $\chi$ ) ( $10^6 \text{ m}^2 \text{ s}^{-1}$ ) shaded and contoured every  $-1 \text{ m}^2 \text{ s}^{-1}$  starting at 0 with irrotational wind vectors to show divergence.

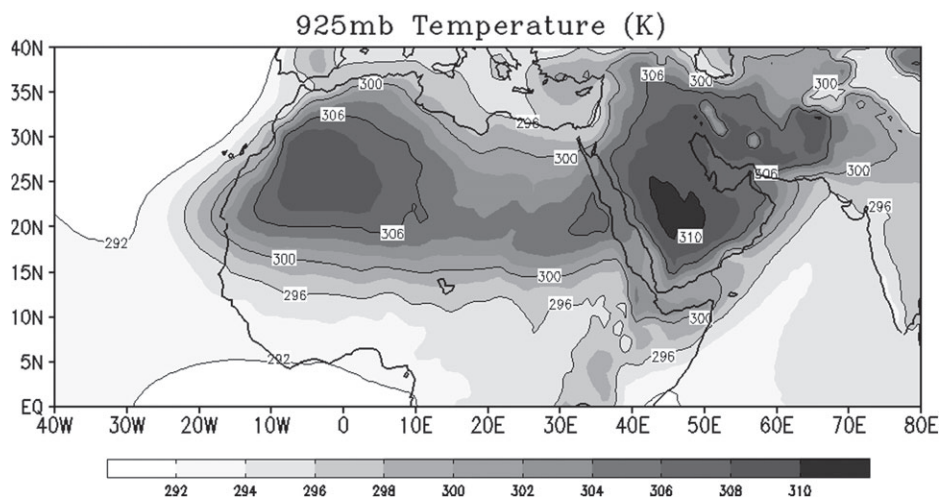


Figure 5. August 32-year (1979–2010) average of 925 mb temperature (K) shaded every 2 K and contoured every 4 K.

#### 4.2. Characteristics and formation of the $\text{LWM}_E$ and $\text{LWM}_W$

Figure 6(a) depicts the potential vorticity field over North Africa at 600 mb. The intensity of the north–south potential vorticity gradients increases from east to west starting around  $40^\circ\text{E}$ . This is directly correlated with the growth of the AEJ and AEWs from the potential vorticity gradient. In Figure 6(b), the reversal of the meridional potential temperature gradient can be seen between 600 and 500 mb levels for both LWMs. The AEJ is a response to the surface baroclinicity and reversal of the temperature gradient that displaces the AEJ in the mid-troposphere (Burpee, 1972; Cook, 1999; Thorncroft and Blackburn, 1999). The dynamics of this have been well observed in previous literatures for the  $\text{LWM}_W$ . Similar dynamical processes hold true for the  $\text{LWM}_E$  except that the  $\text{LWM}_E$  is displaced at slightly higher levels around 550 mb, but is still present at 600 mb. This includes the Darfur Mountains between  $20^\circ$

and  $25^\circ\text{E}$ , the northern portion of the Ethiopian Highlands between  $35^\circ$  and  $40^\circ\text{E}$ , and the Asir Mountains between  $43^\circ$  and  $50^\circ\text{E}$ . The TEJ in the upper atmosphere around 100 mb also exhibits the same dynamics as the AEJ with the negative meridional potential vorticity gradient and reversal of the meridional potential temperature gradient.

In the literature, the anticyclonic systems have been presented using streamfunction to show circulation. The negative meridional gradient of streamfunction (not shown) will result in zonal wind with near real zonal wind estimations for the AEJ. In this study, we want to show how close the zonal geostrophic winds are to real zonal wind using the thermal wind relationship because the understanding of it will help distinguish the differences of the  $\text{LWM}_E$  and the  $\text{LWM}_W$ .

The baroclinicity is strong in West Africa, East Africa, and the Arabian Peninsula (Figure 7(a)), but the  $\text{LWM}_E$  is weaker and smaller than the  $\text{LWM}_W$ . This raises the

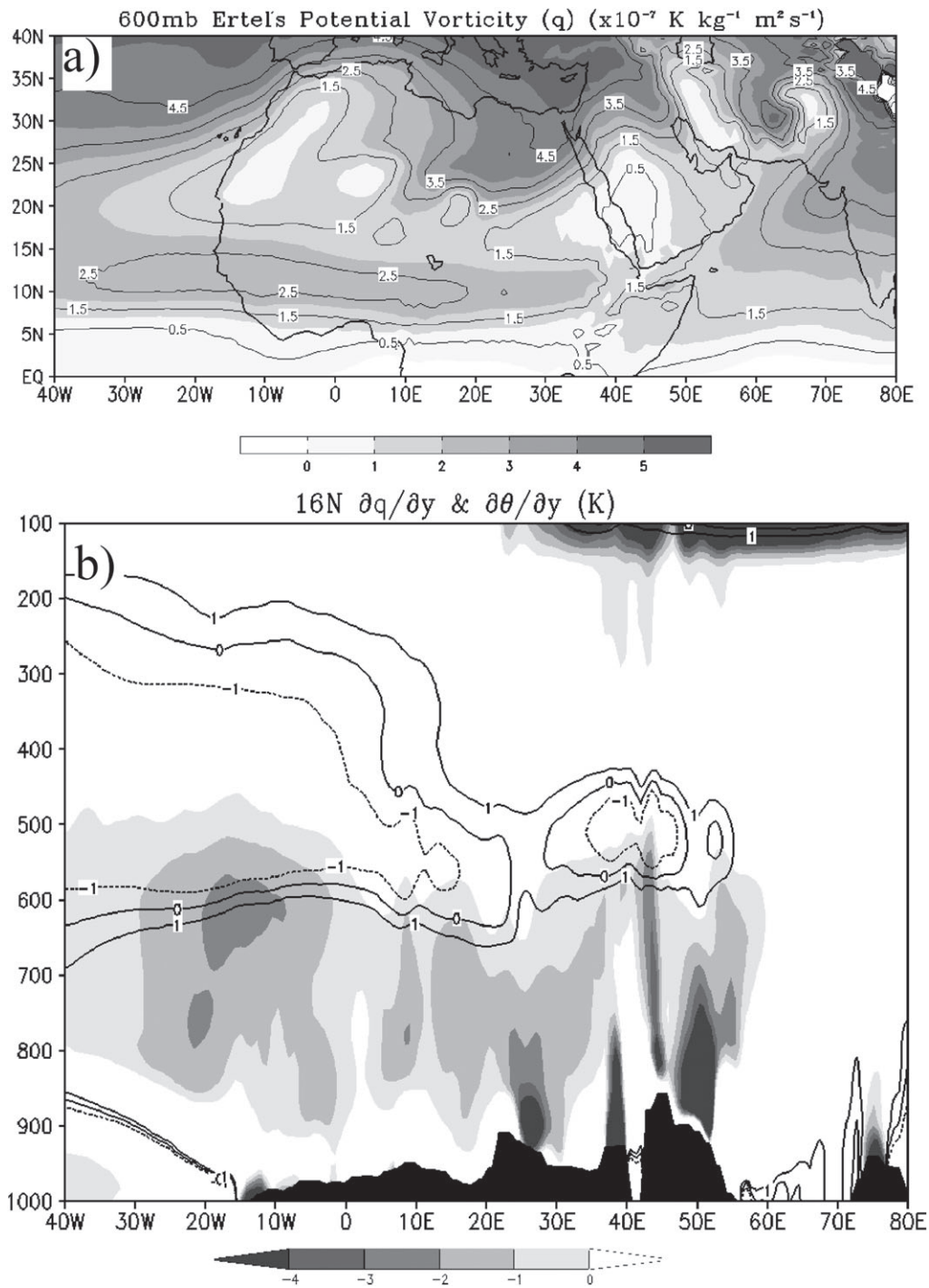


Figure 6. August 32-year (1979–2010) average of (a) 600 mb Ertel's potential vorticity ( $\times 10^{-7} \text{ K kg}^{-1} \text{ m}^2 \text{ s}^{-1}$ ) field shaded every  $1 \text{ K kg}^{-1} \text{ m}^2 \text{ s}^{-1}$  from 1 to  $5 \text{ K kg}^{-1} \text{ m}^2 \text{ s}^{-1}$  and contoured every  $1 \text{ K kg}^{-1} \text{ m}^2 \text{ s}^{-1}$  from 0.5 to  $5.5 \text{ K kg}^{-1} \text{ m}^2 \text{ s}^{-1}$ , (b) vertical cross section at  $16^\circ\text{N}$  of the meridional potential vorticity gradient (shaded) and meridional potential temperature gradient (K) [contours] with a contour interval of  $[-1, 0, 1]$ .

question we want to address: Why is the  $\text{LWM}_E$  weaker than the  $\text{LWM}_W$ ? We hypothesize that the intensity of the weak  $\text{LWM}_E$  is caused by a weak mid-tropospheric high. Figure 7(b) illustrates the connection with the geostrophic wind maxima, which are associated with the Saharan High and Arabian High induced meridional geopotential gradients, respectively. The LWMs are located around 600 and 550 mb directly over the zonal geostrophic maxima in West Africa and East Africa. As the Saharan High is more

intense and broader than the Arabian High, the Saharan High produces a much stronger meridional geopotential gradient in West Africa, thus making the  $\text{LWM}_W$  stronger than the  $\text{LWM}_E$ . The AEJ will be formed at 600 mb with an elongated easterly zonal geostrophic flow generated from baroclinicity. The presence of the Saharan and Arabian Highs will increase easterly flow to the south of the anticyclonic centres because of the increased meridional geopotential gradient. This geopotential gradient along with the

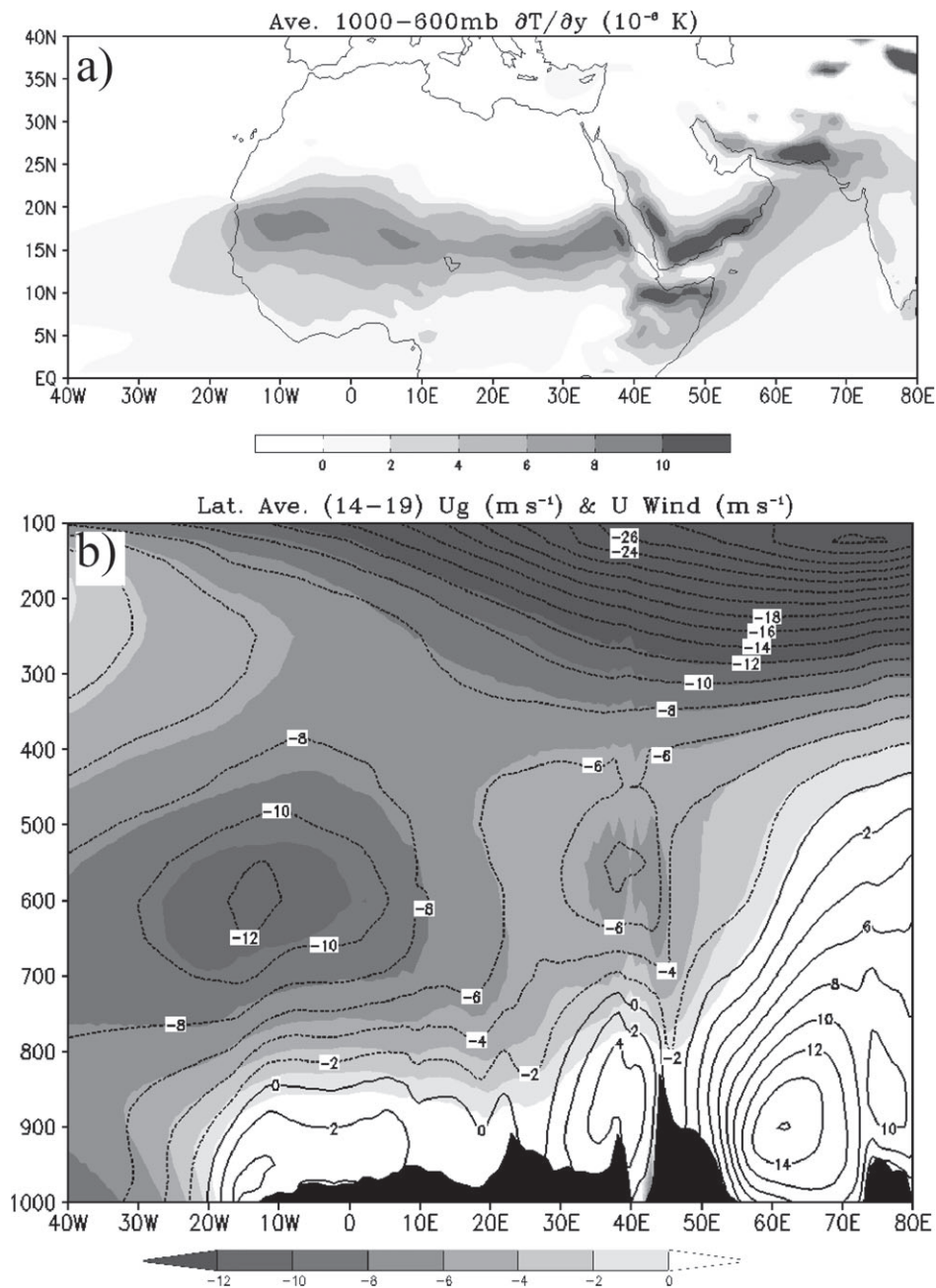


Figure 7. August 32-year (1979–2010) average of (a) the meridional temperature gradient ( $10^{-4}$  K) averaged between 1000–600 mb shaded every 2 K starting at 0 and meridional geopotential gradient contoured every 1 gmp starting at 0, and (b) vertical cross section between 14° and 19°N of geostrophic wind ( $m s^{-1}$ ) shaded every  $-2 m s^{-1}$  starting at 0 and zonal wind ( $m s^{-1}$ ) contoured every  $2 m s^{-1}$ . The terrain is crossed at 16°N.

dominant influence from baroclinicity helps give the AEJ two distinct zonal maxima in East and West North Africa. The geostrophic wind maximum explains the locations of the  $LWM_E$  and  $LWM_W$ .

The local easterly zonal wind extends into the Arabian Peninsula along with a strong meridional temperature gradient, but a weakened meridional geopotential gradient. There is no LWM present over the Arabian Peninsula region. The AEJ decreases in intensity as a result of the meridional geopotential gradient decreasing, but the meridional temperature gradient remains intense across the southern Arabian Peninsula primarily because of the land-sea temperature contrast.

#### 4.3. Case study for 2006: evolution of the anticyclones and LWMs

In the following, we will be looking at the LWM's dynamics over a 32-year period for August to a smaller time scale for 2006 while highlighting August for a 6-hourly time scale analysis. It is important to observe evolution of synoptic features to examine when the  $LWM_E$  is formed.

Figure 8 emphasizes the correlation of the Saharan High/ $LWM_W$  and Arabian High/ $LWM_E$  using daily averages for the entire year of 2006. The maximum geopotential and zonal wind values are calculated for each variable respectively in West Africa and East Africa

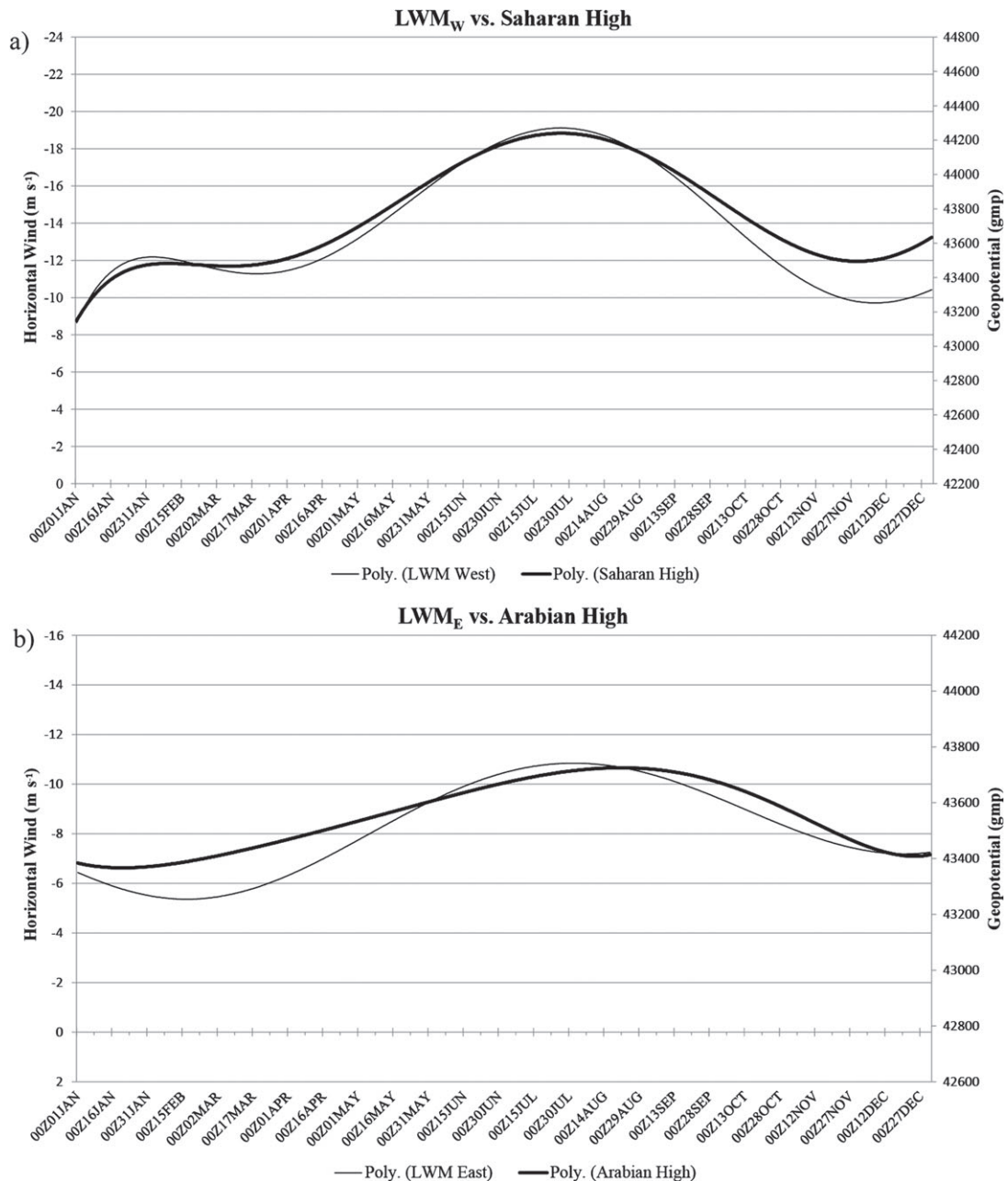


Figure 8. 2006 daily averaged curve of maximum zonal wind ( $\text{m s}^{-1}$ ) (thin line) and geopotential (gmp) (bold line) for (a) the Saharan High/LWM<sub>W</sub> and (b) the Arabian High/LWM<sub>E</sub>.

into the Arabian Peninsula. The results indicate how the LWM<sub>W</sub> and LWM<sub>E</sub> intensities are dependent on the strength of the anticyclonic induced pressure gradient. Figure 8(a) shows strong positive correlation (0.80) of the Saharan High and LWM<sub>W</sub>. The intensity of the LWM<sub>W</sub> fluctuates with the Saharan High intensity. As the Saharan High and LWM<sub>W</sub> are present all year long, the variation of intensity occurs simultaneously. The LWM<sub>E</sub> and Arabian High are not present all year. The correlation (0.70) of the LWM<sub>E</sub> and Arabian High is weak throughout the year, until May. In Figure 8(b), the LWM<sub>E</sub> has an increase in strength, as well as the Arabian High during mid-summer and begins to decrease in the fall (September, October, and November).

The formation and evolution of the LWM<sub>E</sub> and Arabian High are depicted in the monthly averages of 2006 using 600 mb zonal winds and streamfunction (Figure 9). During the winter month of January, the subtropical high stretches from the Africa to India with a jet maximum located to the south of each anticyclonic centre. Over Africa, the LWM<sub>W</sub> exists between 5° and 10°N with no presence of the LWM<sub>E</sub> in East Africa or Arabian High over the Arabian Peninsula. In March and April, the Arabian High begins its formation stage. In May, the Saharan High centre is displaced poleward and a secondary anticyclonic centre forms over the Arabian Peninsula along with the LWM<sub>E</sub>, which reaches the mature stage of the Arabian High. The coexistence of the LWM<sub>E</sub> and Arabian High

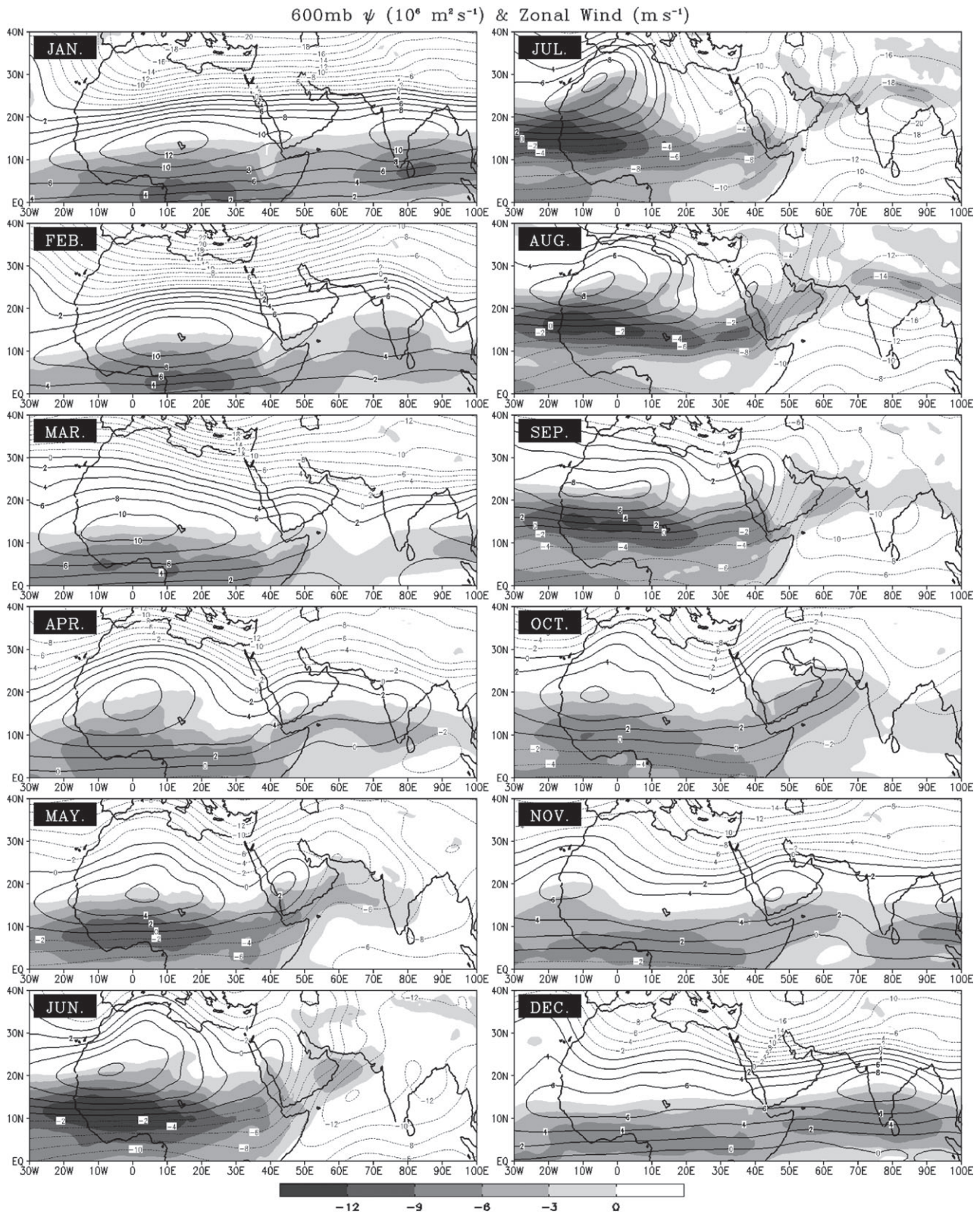


Figure 9. 2006 monthly averages of 600 mb streamfunction ( $\text{m}^2 \text{s}^{-1}$ ) contours and zonal wind ( $\text{m s}^{-1}$ ) shaded every  $3 \text{ m s}^{-1}$ .

indicates that both systems are formed during this time. In June, the Saharan High and  $\text{LWM}_W$  occupy most of North Africa while stretching into East Africa and part of North Arabia. There is no  $\text{LWM}_E$  present during June and July according to the monthly averages of streamfunction

and zonal wind. This is due to the Arabian High being very weak and unable to produce a geopotential gradient to form the  $\text{LWM}_E$ . In August, a second anticyclonic centre develops over the Arabian Peninsula. The development of the Arabian anticyclonic centre induces the  $\text{LWM}_E$  by

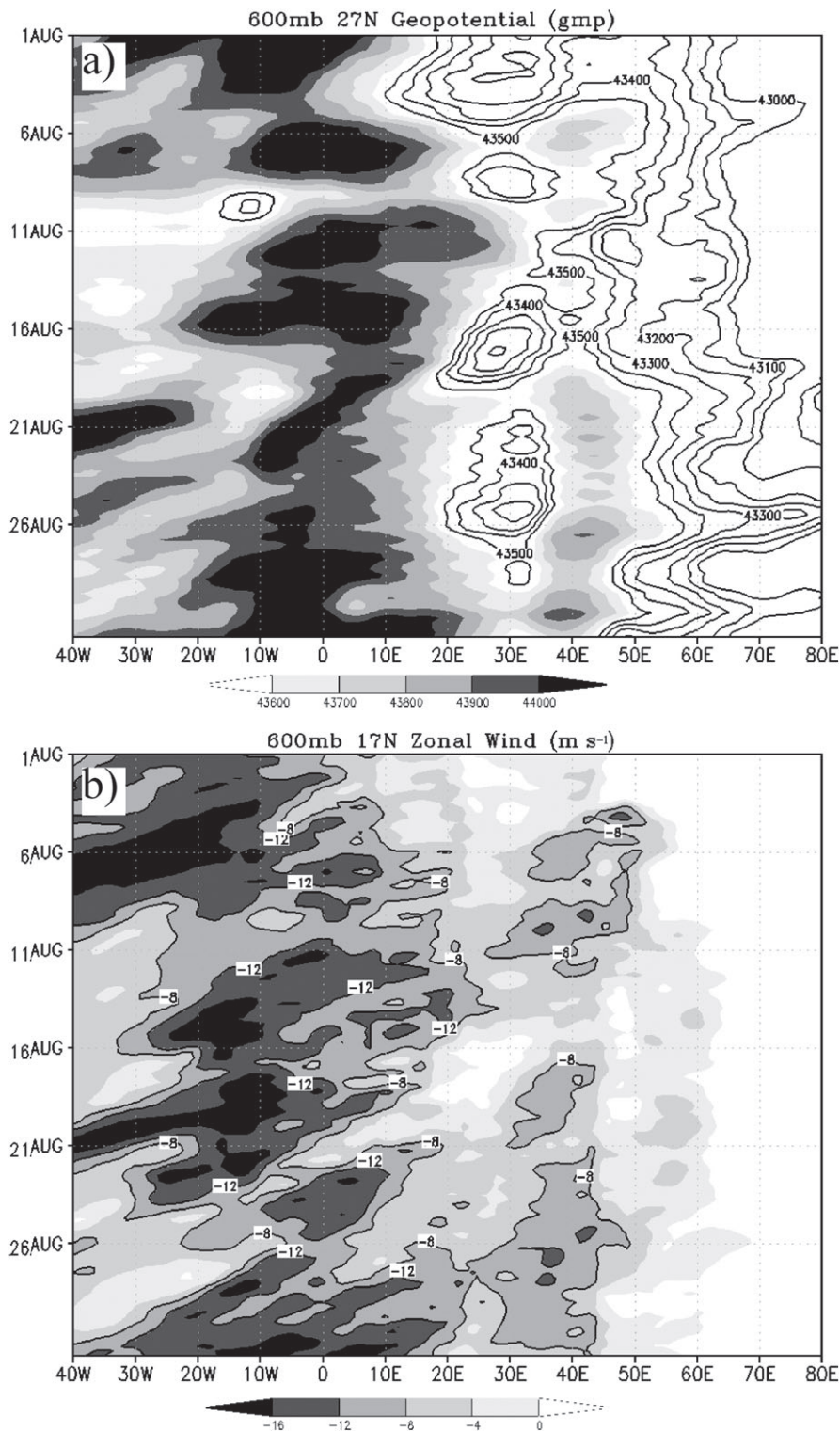


Figure 10. August 2006 Hovmöller diagram of (a) geopotential (gmp) at 27°N shaded between 43 600 and 44 000 every 100 gmp and contoured between 43 000 and 43 500 every 100 gmp and (b) zonal wind (m s<sup>-1</sup>) at 17°N shaded -16 to 0 every -4 m s<sup>-1</sup> and contours for 12 and 8 m s<sup>-1</sup>.

forming from the meridional geopotential gradient. By October, the Saharan High is weakened along with the LWM<sub>W</sub> and the Arabian High is dominant over the Arabian Peninsula.

The Saharan High/LWM<sub>W</sub> and Arabian High/LWM<sub>E</sub> in August are depicted by a Hovmöller diagram every 6 h (Figure 10). The latitudinal cross section for

geopotential and zonal wind are based on their location during August 2006 (Figure 9). The AEJ is on the southern rim of the subtropical anticyclones, so the latitudinal cross section of geopotential is at 27°N (Figure 10(a)) and the latitudinal cross section of zonal wind is at 17°N (Figure 10(b)). In August, the highest geopotential values are located between 20°W and 20°E, which is

directly related to the Saharan High and between 40° and 50°E, which is directly related to the Arabian High. In between these highs is a trough that is associated with the subtropical westerly jet stream over the Mediterranean region (Gaetani *et al.*, 2011). Observations from the Hovmoller diagram of geopotential, the Saharan High shows propagation between August 11 and 21. The zonal wind in Figure 10(b) can be compared with Figure 10(a) to see the relationship of the easterly winds and the high pressure systems. On a 6 hourly time scale, the LWMs can respectively be depicted in the same region of the high pressure systems. As the Hovmoller diagram does not consist of any averaging, the LWMs reach zonal magnitudes higher than the climate average presented in Section 2. The LWM<sub>W</sub> has a zonal wind speed of 16 m s<sup>-1</sup> or greater and the LWM<sub>E</sub> has a zonal wind speed of 10 m s<sup>-1</sup> or greater.

## 5. Conclusion

The AEJ was analysed for the month of August between 1976 and 2010 as well as 2006 as a case study to demonstrate a second maximum core located in East Africa centred at 15°N, 35°E. Once this maximum was identified, there was a series of examinations that explained the dynamical interactions of the LWM<sub>E</sub> and the East African synoptic circulations. Similar to the LWM<sub>W</sub> found and discussed in previous studies, the LWM<sub>E</sub> exhibited very similar mechanisms in formation and maintenance. The LWM<sub>E</sub> is located to the south of the Arabian High much like the LWM<sub>W</sub> located to the south of the Saharan High. The increased intensity of the LWMs associated with AEJ is due to the maximum meridional geopotential gradient from the Saharan and Arabian Highs, which causes the AEJ to be mainly geostrophic. This was explained utilizing the thermal wind relationship to differentiate between the LWM<sub>W</sub> and LWM<sub>E</sub>.

The formation and maintenance of the Saharan and Arabian Highs was also discussed. From the east–west circulation, there are two distinct divergence flows in the mid levels that are located over Africa and the Arabian Peninsula. The upward vertical motion is associated with the ITF heating in which the Saharan and the Arabian thermal lows are located. The rising of warm air converges with the sinking cooler air forming divergence centres over Africa and the Arabian Peninsula. This differential heating from the divergent centres help maintain the anticyclones.

The LWMs and anticyclonic systems were investigated on a smaller spatial time scale for the year 2006 using monthly averages. The formation and evolution of the Arabian High begins in March reaching peak intensity in May, August, and October and the LWM<sub>E</sub> is at maximum intensity during August.

The presence of the LWM<sub>E</sub> can offer better understanding of rainfall distribution and interactions with easterly wave maintenance and propagation in East Africa. More research is needed to understand this interaction, such as high resolution numerical modelling. Climate variability

of the Arabian High and LWM<sub>E</sub> can also be investigated with the El Niño Southern-Oscillation (ENSO) to determine weather changes over East Africa.

## Acknowledgements

We would like to thank Dr Solomon Bililign, the Director of NOAA ISET Center, for his continuous encouragement in pursuing this study. Comments made by three anomalous reviewers, Dr Jin Lee at NOAA ESRL, Dr Bo-Wen Shen at University of Maryland and Dr Jing Zhang at NC A&T State University are highly appreciated. This research was supported by the National Oceanic and Atmospheric Administration Educational Partnership Program under Cooperative Agreement No: NA06OAR4810187 (2006–2012) and by the National Science Foundation Award AGS-1265783.

## References

- Burpee RW. 1972. The origin and structure of easterly waves in the lower troposphere of North Africa. *J. Atmos. Sci.* **29**: 77–90.
- Chen T-C. 2005. Maintenance of the mid tropospheric North African summer circulation: Saharan high and African easterly jet. *J. Clim.* **18**: 2943–2962.
- Chen T-C. 2006. Characteristics of African easterly waves depicted by ECMWF Reanalysis for 1991–2000. *Mon. Weather Rev.* **134**: 3539–3566.
- Cook KH. 1999. Generation of the African easterly jet and its role in determining West African precipitation. *J. Clim.* **12**: 1165–1184.
- Dee DP, Uppala SM, Simmons AJ, Berrisford P, Poli P, Kobayashi S, Andrae U, Balmaseda MA, Balsamo G, Bauer P, Bechtold P, Beljaars ACM, van de Berg L, Bidlot J, Bormann N, Delsol C, Dragani R, Fuentes M, Geer AJ, Haimberger L, Healy SB, Hersbach H, Hólm EV, Isaksen L, Kållberg P, Köhler M, Matricardi M, McNally AP, Monge-Sanz BM, Morcrette JJ, Park BK, Peubey C, de Rosnay P, Tavolato C, Thépaut JN, Vitart F. 2011. The ERA-Interim reanalysis: configuration and performance of the data assimilation system. *Q. J. R. Meteorol. Soc.* **137**: 553–597.
- Dezfuli AK, Nicholson SE. 2010. A note on long term variations of the African easterly jet. *Int. J. Climatol.* **31**: 2049–2054, DOI: 10.1002/joc.2209.
- Gaetani M, Baldi M, Dalu GA, Maracchi G. 2011. Jetstream and rainfall distribution in the Mediterranean region. *Nat. Hazards Earth Syst. Sci.* **11**: 1–14, DOI: 10.5194/nhess-11-1-2011.
- Grist JP, Nicholson SE, Barcilon AL. 2002. Easterly wave over Africa. Part II: observed and modeled contrast between wet and dry years. *Mon. Weather Rev.* **130**: 212–225.
- Holton JR. 2004. *An Introduction to Dynamic Meteorology*, 4th edn. Elsevier Academic Press: Amsterdam.
- Hurlburt HE, Dana Thompson J. 1976. A numerical model of the Somali current. *J. Phys. Oceanogr.* **6**: 646–664.
- Kalnay E, Kanamitsu M, Kistler R, Collins W, Deaven D, Gandin L, Iredell M, Saha S, White G, Woollen J, Zhu Y, Leetmaa A, Reynolds R, Chelliah M, Ebisuzaki W, Higgins W, Janowiak J, Mo KC, Ropelewski C, Wang J, Jenne R, Joseph D. 1996. The NCEP/NCAR 40-year reanalysis project. *Bull. Am. Meteorol. Soc.* **77**: 437–471.
- Lavaysse C, Flamant C, Janicot S, Parker DJ, Lafore J-P, Sultan B, Peloni J. 2009. Seasonal evolution of the West African heat low: a climatological perspective. *Clim. Dyn.* **33**: 313–330, DOI: 10.1007/s00382-009-0553-4.
- Lavaysse C, Flamant C, Janicot S, Knippertz P. 2010. Links between African easterly waves, midlatitude circulation and intraseasonal pulsations of the West African heat low. *Q. J. R. Meteorol. Soc.* **136**: 141–158, DOI: 10.1002/qj.555.
- Lin Y-L, Liu L, Tang G, Spinks J, Jones W. 2013. Origin of the pre-Tropical Storm Debby (2006) African easterly wave-mesoscale convective system. *Meteorol. Atmos. Phys.* **120**: 123–144, DOI: 10.1007/s00703-013-0248-6.

- Parker DJ, Thorncroft CD, Burton RR, Diongue-Niang A. 2005. Analysis of the African easterly jet using aircraft observations from the JET2000 experiment. *Q. J. R. Meteorol. Soc.* **131**(608): 1461–1482.
- Rao PG, Hatwar HR, Al-Sulaiti HH, Al-Mulia AH. 2003. Summer Shamals over the Arabian Gulf. *Weather* **58**: 472–478.
- Reed RJ, Norquist DC, Recker EE. 1977. The structure and properties of African wave disturbances as observed during Phase III of GATE. *Mon. Weather Rev.* **105**: 317–333.
- Saha S, Nadiga S, Thiaw C, Wang J, Wang W, Zhang Q, Van den Dool HM, Pan HL, Moorthi S, Behringer D, Stokes D, Pena M, Lord S, White G, Ebisuzaki W, Xie P. 2006. The NCEP climate forecast system. *J. Clim.* **19**: 3483–3517.
- Thorncroft CD, Blackburn M. 1999. Maintenance of the African easterly jet. *Q. J. R. Meteorol. Soc.* **125**: 763–786.
- Thorncroft CD, Parker DJ, Burton RR, Diop M, Ayers JH, Barjat H, Devereau S, Diongue A, Dumelow R, Kindred DR, Price NM, Saloum M, Taylor CM, Tompkins AM. 2003. The Jet2000 Project: aircraft observations of the African easterly jet and African easterly waves. *Bull. Am. Meteorol. Soc.* **84**: 337–351.
- Uppala SM, Kållberg PW, Simmons AJ, Andrae U, Bechtold VDC, Fiorino M, Gibson JK, Haseler J, Hernandez A, Kelly GA, Li X, Onogi K, Saarinen S, Sokka N, Allan RP, Andersson E, Arpe K, Balmaseda MA, Beljaars ACM, Berg LVD, Bidlot J, Bormann N, Caires S, Chevallier F, Dethof A, Dragosavac M, Fisher M, Fuentes M, Hagemann S, Hólm E, Hoskins BJ, Isaksen L, Janssen PAEM, Jenne R, McNally AP, Mahfouf JF, Morcrette JJ, Rayner NA, Saunders RW, Simon P, Sterl A, Trenberth KE, Untch A, Vasiljevic D, Viterbo P, Woollen J. 2005. The ERA-40 re-analysis. *Q. J. R. Meteorol. Soc.* **131**: 2961–3012, DOI: 10.1256/qj.04.176.
- Wu M-LC, Reale O, Schubert SD, Suarez MJ, Koster RD, Pegion PJ. 2009. African easterly jet: structure and maintenance. *J. Clim.* **22**: 4459–4480.